Propargyl Radical: Ab Initio Anharmonic Modes and the Polarized Infrared Absorption Spectra of Matrix-Isolated $HCCCH_2$

Evan B. Jochnowitz,[†] Xu Zhang,[†] Mark R. Nimlos,*[,†,‡] Mychel E. Varner,[§] John F. Stanton,*[,§] and G. Barney Ellison*[,†]

Department of Chemistry and Biochemistry, University of Colorado, Boulder, Colorado 80309-0215, National Renewable Energy Laboratory, 1617 Cole Blvd., Golden, Colorado 80401, and Institute for Theoretical Chemistry, Department of Chemistry, University of Texas, Austin, Texas 78712

Received: November 15, 2004

The propargyl radical has twelve fundamental vibrational modes, $\Gamma_{vib}(HCCCH_2) = 5a_1 \oplus 3b_1 \oplus 4b_2$, and nine have been detected in a cryogenic matrix. Ab initio coupled-cluster anharmonic force field calculations were used to help guide some of the assignments. The experimental $HC{\equiv}C{\cdots}CH_2$ matrix frequencies (cm^{-1}) and polarizations are a_1 modes—3308.5 ± 0.5, 3028.3 ± 0.6, 1935.4 ± 0.4, 1440.4 ± 0.5, 1061.6 ± 0.8; b_1 modes—686.6 ± 0.4, 483.6 ± 0.5; b_2 modes—1016.7 ± 0.4, 620 ± 2. We recommend a complete set of gas-phase vibrational frequencies for the propargyl radical, $HC{\equiv}C{\cdots}CH_2$ $\tilde{X}$ $^2B_1$. From an analysis of the vibrational spectra, the small electric dipole moment, $\mu_D(HCCCH_2) = 0.150$ D, and the large resonance energy ($HCCCH_2$), roughly 11 kcal mol^{-1}, we conclude that propargyl is a completely delocalized hydrocarbon radical and is best written as $HC{\equiv}C{\cdots}CH_2$.

I. Introduction

The propargyl[1] radical, $HCCCH_2$, is one of the simpler conjugated hydrocarbon radicals. In addition to being interesting in its own right, propargyl is believed[2] to be a direct precursor of aromatic species in flames: $HCCCH_2 + HCCCH_2 \rightarrow C_6H_6$ (benzene). In this paper we report the infrared spectrum of the propargyl radical. Using a heated supersonic or hyperthermal nozzle we are able to prepare matrix isolated propargyl radicals. A Fourier transform infrared (FTIR) spectrometer was used to measure the infrared absorption spectra of these matrix isolated radicals. Polarized 248 nm light from a KrF excimer laser was used to orient the propargyl radicals so we can measure the linear dichroism (LD) spectra of photooriented samples. The LD spectra enable us to establish experimental polarizations of most of the vibrational bands. We have measured the infrared absorption spectra of propargyl radicals and have identified 9 of the 12 fundamental vibrational modes. To analyze these spectra, we have determined the potential energy and dipole moment surfaces of the $HCCCH_2$ $\tilde{X}$ $^2B_1$ radical with coupled-cluster theory. CCSD(T) calculations are used to analyze the molecular structure, spin density, and electric dipole moment. The combination of the experimental vibrational frequencies, the measured polarizations, and the CCSD(T) anharmonic frequencies permits a relatively straightforward assignment of the vibrational spectrum of the propargyl radical.

Early EPR spectroscopy[3] revealed propargyl to be a radical with C_{2v} symmetry. The observed hyperfine splitting pattern revealed a "doublet of triplets" with comparable spin densities [(spin)(atom)$^{-1}$] on the (1,3) carbons.

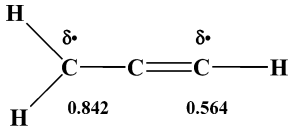

(1)

The EPR spectrum indicates that neither $^{\bullet}CH_2{-}C{\equiv}CH$ nor $CH_2{=}C{=}CH^{\bullet}$ is good representation of this radical and we will use the symbol $HC{\equiv}C{\cdots}CH_2$ to represent propargyl.

Fourier transform microwave spectroscopy[4] has been used to measure propargyl's ground-state rotational constants: $A_0 =$ 288 055.0 MHz, $B_0 = 9523.6775 \pm 0.0060$ MHz, and $C_0 = 9206.8805 \pm 0.0060$ MHz. The inertial defect, $\Delta = (I_{cc} - I_{aa} - I_{bb})$, was measured to be 0.067 797 ± 0.000 075 amu Å^2, which implies that the radical must be planar (or nearly so). However, the microwave analysis did not touch upon any isotopomers; consequently, no structural information was determined. Stark spectra of propargyl radical deposited in helium nanodrops were analyzed[5] to find the electric dipole moment of the radical, $|\mu_D(HCCCH_2)| = 0.150 \pm 0.005$ D.

More than a decade ago, it was demonstrated[6] that a hyperthermal nozzle could decompose propargyl bromide to produce intense beams of the radical.

$$HC{\equiv}C{-}CH_2{-}Br + \Delta \rightarrow HC{\equiv}C{\cdots}CH_2 + Br \qquad (2)$$

Photoionization with a VUV laser ($\lambda_0 = 118.2$ nm or 10.487 eV) yielded the ionization potential ($HCCCH_2 + \hbar\omega_{118.2nm} \rightarrow HCCCH_2^+ + e^-$). The ionization energy of propargyl radical was found to be $IE(HC{\equiv}C{\cdots}CH_2) = 8.67 \pm 0.02$ eV.

Photodetachment experiments[7,8] with the allenyl anion ($CH_2{=}C{=}CH^- + \hbar\omega_{351nm} \rightarrow HC{\equiv}C{\cdots}CH_2 + e^-$), provided the electron affinity of propargyl radical, $EA(HC{\equiv}C{\cdots}CH_2) = 0.918 \pm 0.008$ eV. Flowing afterglow/selected ion flow tube studies of the ion chemistry of $CH_2{=}C{=}CH^-$ were used to

* Corresponding authors. E-mail: G.B.E., barney@jila.colorado.edu; M.R.N., mark_nimlos@nrel.gov; J.F.S., jfstanton@mail.utexas.edu.
[†] University of Colorado.
[‡] National Renewable Energy Laboratory.
[§] University of Texas.

10.1021/jp040719j CCC: $30.25
Published on Web 04/08/2005

TABLE 1: Earlier Studies of $HCCCH_2$ Vibrational Modes

mode		description	ν/cm^{-1}	conditions	ref
a_1	1	CH_2CC-H st	3322.2929 ± 0.0020	CW color center laser spectrospy	17, 18
			3322.15 ± 0.01	CW color center laser spectrospy/He nanodrops	5
			3310	N_2 matrix	13
			3308.8	Ar matrix	15
			3307	Ar matrix	14
	2	sym H_2C-CCH st	3026	Ar matrix	14
	3	$CH_2C=CH \oplus CH_2\cdots CCH$ st	2080	Ar matrix	14
	4	$H_2C\cdots CCH$ scissors	1440	Ar matrix	14
	5	$CH_2\cdots CCH$ st	1017	Ar matrix	14
b_1	6	$H_2C\cdots CCH$ umbrella	687.17603 ± 0.00062	time resolved IR diode laser spectroscopy	16
			688	N_2 matrix	13
			618	Ar matrix	14
	7	CH_2CC-H out-of-plane bend	490 ± 10	$CH_2=C=CH^-$ photodetachment	7, 8
			532	Ar matrix	14
	8	$CH_2\cdots C=CH$ out-of-plane bend	na		
b_2	9	asym $H_2C\cdots CCH$ st	3111	Ar matrix	14
	10	$H_2C\cdots CCH \oplus H_2C-C\equiv CH$ in-plane bend	1062	Ar matrix	14
	11	CH_2CC-H in-plane bend	647.3	time resolved IR diode laser spectroscopy	16
			686	Ar matrix	14
	12	$H_2C\cdots C=CH$ in-plane bend	482	Ar matrix	14
			484	N_2 matrix	13
			483.5	Ar matrix	15

measure the enthalpy of deprotonation of $HC\equiv CCH_3$; $\Delta_{acid}H_{298}(HCCCH_2-H \rightarrow CH_2=C=CH^- + H^+) = 383 \pm 3$ kcal mol^{-1}. The negative ion/acidity thermochemical cycle[9-11] relates the acidity, electron affinity, and bond dissociation energy: $\Delta_{acid}H_{298}(R-H) = DH_{298}(R-H) + IE(H) - EA(R)$. The measured $EA(HC=C\cdots CH_2)$ and $\Delta_{acid}H_{298}(HCCCH_2-H)$ values yielded[8] the bond enthalpy[12] of methylacetylene, $DH_{298}(HCCCH_2-H) = 90 \pm 3$ kcal mol^{-1}, and the absolute heat of formation of the propargyl radical, $\Delta_fH_{298}(HC=C\cdots CH_2\ \tilde{X}\ ^2B_1) = 83 \pm 3$ kcal mol^{-1}.

Table 1 is a summary of previous experimental results. In pioneering studies[13] by Jacox and Milligan, several of the fundamentals of $HC=C\cdots CH_2$ were detected in a nitrogen matrix at 14 K. Subsequent work[14,15] extended the matrix studies to assign most of propargyl's fundamentals although there is some confusion about the ν_6, ν_7, and ν_{11} modes. The strong $^{H}_{H}\rangle C=CCH$ umbrella mode (of b_1 symmetry) was detected[16] by time-resolved IR diode laser spectroscopy in a free jet at $\nu_6 = 687.17603 \pm 0.00062$ cm^{-1}. The intense $H-CCCH_2$ stretching mode was also detected[17,18] in a free jet by CW color center laser spectroscopy at $\nu_1 = 3322.2929 \pm 0.0020$ cm^{-1}; the $\nu_1(D\text{-}CCCH_2)$ frequency was measured[19] to be 2557.33_7 cm^{-1}. When propargyl radical was isolated in a helium nanodroplet,[5] this CH band shifted slightly to 3322.15 ± 0.01 cm^{-1}. Negative ion photoelectron spectroscopy[7,8] of mass-selected beams of the $CH_2=C=CH^-$ ion revealed a long progression of the CH_2CC-H out-of-plane b_1 mode at $\nu_7 = 490 \pm 10$ cm^{-1}.

In addition to its vibrational spectroscopy, the electronic spectra of the propargyl radical has been examined. Flash photolysis[20] of $HC\equiv C-CH_2Br$, $HC\equiv C-CH_2Cl$, $HC\equiv C-CH_3$, and $CH_2=C=CH_2$ produced the $HC=C\cdots CH_2$ radical. There are two, nearly degenerate states that arise from the $\pi_x \leftarrow \pi_y$ and $\pi_x \leftarrow \pi_x$ transitions from the $\tilde{X}\ ^2B_1\ |1a_1^2\ 2a_1^2\ 3a_1^2\ 4a_1^2\ 5a_1^2\ 6a_1^2\ 7a_1^2\ 1b_2^2\ 1b_1^2\ 2b_2^2\ 2b_1^1\rangle$ state. The lowest-lying electronic states are nominally $|\tilde{A}\ ^2B_2\rangle = |1a_1^2\ 2a_1^2\ 3a_1^2\ 4a_1^2\ 5a_1^2\ 6a_1^2\ 7a_1^2\ 1b_2^2\ 1b_1^2\ 2b_2^1\ 2b_1^2\rangle$ and $|\tilde{B}\ ^2B_1\rangle = |1a_1^2\ 2a_1^2\ 3a_1^2\ 4a_1^2\ 5a_1^2\ 6a_1^2\ 7a_1^2\ 1b_2^2\ 1b_1^1\ 2b_2^2\ 2b_1^2\rangle$. The $\tilde{A} \leftarrow \tilde{X}$ transition is forbidden because the electronic transition moment transforms like A_2 under C_{2v} symmetry; however, $\tilde{B} \leftarrow \tilde{X}$ will be strongly allowed. MCSCF calculations[21] predict that deformation of the CH_2CC-H bond out of the molecular plane will lower the symmetry of the $\tilde{A}$ state of propargyl to $^2A''$ and the $\tilde{B}$ state becomes $^2A'$.

In the 1960s a transition was found at 290−345 nm that was rotationally unstructured, suggesting a dissociative CH_2CCH^* state.[20] More recent experiments clearly show a pair of closely spaced excited states for the propargyl radical.[22] A weak set of bands was assigned as $0_0°(\tilde{A}\ ^2A'' \leftarrow \tilde{X}\ ^2B_1) = 28\ 409$ cm^{-1} (3.52 eV) whereas the stronger set of features was identified as the $0_0°(\tilde{B}\ ^2A' \leftarrow \tilde{X}\ ^2B_1) = 29\ 146$ cm^{-1} (3.61 eV) transition. A third $HC=C\cdots CH_2$ band system has recently been observed[23] in the spectral range of 230−300 nm. This is a relatively broad absorption with a maximum cross section of 1.2×10^{-17} cm^2 molecule^{-1} at 242 nm (5.123 eV or 30 120 cm^{-1}). The electronic transitions in the propargyl radical were calculated by ab initio electronic structure methods using the CASSCF, CASPT2, CIS, and EOM-CCSD techniques; the newly observed band was assigned to the in-plane π^* (b_2) $\leftarrow \pi$ (b_2) allowed transition. Consequently the $\tilde{C}$ $HC=C\cdots CH_2$ state at 230−300 nm was assigned to be of $^2B_1$ symmetry. The femtosecond dynamics of the $\tilde{C}$ state has just been reported.[52]

II. Methods

A. Photoionization Mass Spectrometry and Infrared Spectroscopy. Most matrix-isolated radicals are generally prepared by photodissociation of an appropriate precursor (usually by a laser). However, we produce the propargyl radical in the gas phase by thermally dissociating a suitable precursor molecule in a hyperthermal nozzle, which expands through a supersonic jet.[24] Thermal dissociation nozzles for propargyl radical production have been described earlier.[5,6] Two different precursors were used in this work: $HC\equiv CCH_2Br$ and $HC\equiv CCH_2CH_2ONO$. The propargyl bromide precursor was purchased from Aldrich Chemical Co. whereas butyne nitrite had to be synthesized. The nitrite is a convenient source[25] of propargyl radical because the O−NO bond is so weak; $\Delta H_{298}(HCCCH_2CH_2O-NO) \cong 42$ kcal mol^{-1}.

$$HC\equiv C-CH_2-CH_2-O-N=O + \Delta \rightarrow HC=C\cdots CH_2 + HCHO + NO \quad (3)$$

To optimize radical production, the dosing nozzle was interfaced with a photoionization mass spectrometer (PIMS). The skimmed output of the nozzle was crossed with 118.2 nm (10.487 eV) light from the ninth harmonic of a YAG laser. Molecules with an ionization potential less than 10.5 eV are

ionized and analyzed by a reflectron time-of-flight mass spectrometer. Mass spectra resulting from each precursor were measured as a function of pyrolysis temperature.

The hyperthermal nozzle was mounted to the vacuum shroud of an APD two stage closed-cycle helium cryostat, approximately 2.5 cm away from the cryogenic CsI window. Gas mixtures were created by seeding a precursor in argon. The precursor vapor was collected by de-gassing the precursor liquid at room temperature. The hyperthermal nozzle was operated with approximately a 1.3 ms pulse width and a stagnation pressure of 1.2 atm, with a 1.2 L stagnation reservoir. The pressure drop in the stagnation reservoir was measured using a capacitance monometer to determine the gas throughput.

Radicals were deposited on a CsI salt window cryogenically cooled to 17 K. The infrared spectrum of the sample was measured using a Nicolet Magna 550 Fourier transform infrared spectrometer with a mercury/cadmium/telluride (MCT-A or B) detector. The APD cryostat is equipped with a pair of CsI side windows through which the IR beam from the instrument passes. Polarized IR radiation is generated using a Molectron wire grid IR polarizer.

For each of propargyl's vibrational modes, the integrated infrared intensities, *A*, were monitored as well. Starting with Beer's law, $I(\nu) = I_0(\nu)\exp[-nz\sigma(\nu)]$, the integrated infrared intensity is defined as the integral of the IR absorption cross section over the bandwidth; $A = \int d\nu\ \sigma(\nu)$. Here $I(\nu)$ is the transmitted light intensity, $I_0(\nu)$ the incident light intensity, n the radical concentration (mol dm^{-3}), z the optical path length (cm), and $\sigma(\nu)$ is the infrared absorption cross section (cm^2 molecule^{-1}). *A* formally has the units[26] of km mol^{-1}.

$$A = \frac{1}{nz}\int_{\text{IR band}} d\nu \ln\left|\frac{I_0(\nu)}{I(\nu)}\right| = \int_{\text{IR band}} d\nu\ \sigma(\nu) \qquad (4)$$

As eq 3 indicates, thermal dissociation of butyne nitrite produces propargyl as well as formaldehyde and nitric oxide. If HC≡C⋯CH_2, HCHO, and NO were the only products of the thermal dissociation (3), we could use the known[26] integrated IR intensities of HCHO and NO to extract absolute *A* values for HC≡C⋯CH_2. However, both our PIMS and IR spectra (vide infra) clearly show that in the hyperthermal nozzle some propargyl radicals abstract H atoms to form HC≡C−CH_3 and CH_2=C=CH_2, whereas others dimerize to form benzene. Consequently, there are not equal numbers of HC≡C⋯CH_2, HCHO, and NO and we can only report relative *A* values for propargyl.

B. Chemical Synthesis of Propargyl Radical Precursors. To produce samples of propargyl, butyne nitrite (HC≡CCH_2-CH_2ONO) was synthesized from 3-butyn-1-ol (HC≡CCH_2CH_2-OH) and sodium nitrite ($NaNO_2$). $NaNO_2$ was dissolved in water and mixed with the alcohol, and HCl was added dropwise to the solution. The reaction flask was kept cold with an ice bath. The net reaction produced the nitrite, salt, and water, with the nitrite forming a separate layer in the reaction flask.

The butyne nitrite layer was purified through vacuum distillation, with the product being condensed in a flask kept cold with a dry ice/ethanol bath. The reaction generally produces a high yield. HC≡CCH_2CH_2ONO was stored in a dark freezer to prevent degradation when not in use.

C. Electronic Structure Calculations. Density functional theory is a rapid, reliable computational method to predict the molecular structure, moments of charge, and harmonic vibrational $\{\omega\}_i$ frequencies of many polyatomic organic molecules. We have used a commercial computer program that employs the B3LYP functional, which is a combination of exchange from Becke's three-parameter HF/DFT hybrid exchange functional[27] (B3) with the dynamical correlation functional[28] of Lee, Yang, and Parr (LYP).

Coupled-cluster theory,[29−32] though more expensive than DFT methods, provides a nearly quantitative treatment of electron correlation in most cases and can therefore provide accuracy beyond that achievable with DFT. Accordingly, we have used another package (ACES III) to calculate the equilibrium geometry, anharmonic force field, and dipole moment function for propargyl using the CCSD(T) method[33,34] with an atomic natural orbital (ANO) basis set.[35] Due to relatively strong spin contamination in the unrestricted Hartree−Fock orbitals, we have used the restricted open-shell (ROHF) approach to provide the orbitals. Though analytic first derivatives of ROHF-based CCSD(T) are available,[36] analytic second derivatives have not yet been implemented. Accordingly, the harmonic frequencies and anharmonic force constants needed for estimation of the fundamental, combination and overtone frequencies were calculated using numerical differentiation of analytic gradients using a general approach described elsewhere.[37] Care was taken to ensure that the numerical precision of the frequencies (harmonic and anharmonic) quoted in Table 2 are precise to roughly 1 cm^{-1}. The core molecular orbitals corresponding to the 1s carbon atomic orbitals were excluded from the correlation treatment.

III. Results

The target propargyl radical has twelve vibrational modes; the irreducible representations of the modes are $\Gamma_{vib}(HCCCH_2) = 5a_1 \oplus 3b_1 \oplus 4b_2$. All of these modes are active in the infrared.

A. Electronic Structure Calculations. Table 2 collects the results of our DFT and CCSD(T) calculations for the ground state of propargyl radical;[38] we also tabulate the results of an earlier CEPA-1 calculation.[39] All three methods find the ground state of the radical to be HC≡C⋯CH_2 $\tilde{X}$ $^2B_1$. The CCSD(T) and CEPA-1 methods lead to values of $\mu_D(CH_2CCH)$ that are close to the experimental[5] value of $|\mu_D(CH_2CCH)| = 0.150 \pm 0.005$ D whereas the B3LYP value of 0.07 D is the smallest of these. All computational methods predict the sign of the electric dipole to be $^{\delta+}(CH_2CCH)^{\delta-}$.

B. Optimization of the Propargyl Radical Source. To study the infrared spectroscopy of the HC≡C⋯CH_2 radical in an efficient manner, we have used the PIMS to optimize conditions for radical production. Photoionization mass spectrometric traces for the HC≡CCH_2Br and HC≡CCH_2CH_2ONO precursors are shown in Figures 1 and 2.

In Figure 1 propargyl bromide is thermally dissociated to generate propargyl, eq 2. As the nozzle is heated, Br atoms are not observed because *IE*(Br) is 11.8 eV whereas the VUV laser is only 10.487 eV ($\hbar\omega_{118.2nm}$). Heating the nozzle to 1000 K induces dissociation of propargyl bromide and $HCCCH_2^+$ is clearly observed at *m*/*z* 39. The feature at *m*/*z* 92 belongs to $C_6H_5CH_3^+$, which derives from the toluene stabilizer added to the commercial supply of HC≡CCH_2Br. At a nozzle temperature of 1200 K, two HC≡C⋯CH_2 radicals dimerize to form C_6H_6 *m*/*z* 78. The IR spectra (vide infra) clearly shows that the C_6H_6 adduct is benzene. At higher nozzle temperatures (1400 K), the HC≡C⋯CH_2 radicals are abstracting H atoms in the nozzle and producing CH_2=C=CH_2 and HC≡C−CH_3. Figure 1 shows signals from ions at *m*/*z* 40. The IR spectra (vide infra) permit us to identify both allene and methylacetylene as reaction products.

Figure 2 shows that similar results were obtained when butyne nitrite is thermally dissociated, eq 3. Heating the nozzle to 1000

TABLE 2: Electronic Structure Calculations for CH_2CCH $\tilde{X}$ $^2B_1$

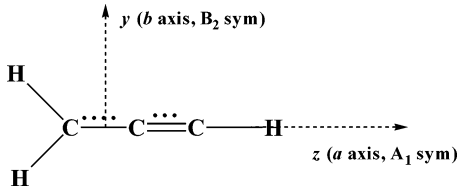

	B3LYP/6-311G(d,p)	CCSD(T)/ANO	CEPA-1/117 cGTO[39]
$r(CH_2CC-H)$/Å	1.062	1.063	1.063
$r(H-CHCCH)$/Å	1.083	1.081	1.080
$r(CH_2C\equiv CH)$/Å	1.222	1.228	1.223
$r(CH_2\cdots CCH)$/Å	1.367	1.380	1.383
θ(H—CHCCH)/deg	120.9	120.5	120.5
$\mu_D{}^{\delta+}(CH_2CCH)^{\delta-}$/D	0.07	0.12	0.14
$\lvert\mu_D(CH_2CCH)\rvert = 0.150 \pm 0.005$ D			ref 5

mode		description	ω/cm^{-1}	A/km mol^{-1}	$\upsilon(\omega)$/cm^{-1}	A/km mol^{-1}	υ/cm^{-1}
a_1	1	CH_2CC-H st	3468	59	3323 (3460)	51	3351
	2	sym $H_2C\cdots CCH$ st	3140	3	3037 (3165)	2	3112
	3	$CH_2C\equiv CH - CH_2\cdots CCH$ st	2011	3	1923 (1983)	6	1951
	4	$H_2\cdots CCH$ scissors	1455	1	1444 (1465)	0	1458
	5	$CH_2C\equiv CH \oplus CH_2\cdots CCH$ st	1090	2	1055 (1058)	4	1049
b_1	6	$H_2C\cdots CCH$ umbrella	682	47	689 (667)	40	
	7	CH_2CC-H out-of-plane bend	468	50	482 (477)	51	
	8	$CH_2-C\equiv CH$ out-of-plane bend	403	5	398 (389)	5	
b_2	9	asym $H_2C\cdots CCH$ st	3230	2	3116 (3266)	0	
	10	$H_2C\cdots CCH \oplus CH_2\cdots C\equiv CH$ in-plane bend	1031	0.4	1018 (1034)	2	
	11	CH_2CC-H in-plane bend	637	52	612 (616)	47	
	12	$CH_2\cdots C\equiv CH$ in-plane bend	352	6	338 (330)	5	

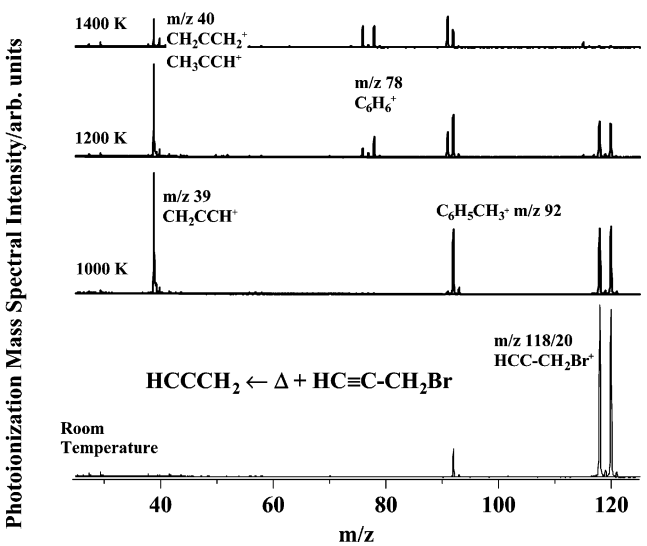

Figure 1. Photoionization mass spectra of the output of the hyperthermal nozzle; $HC\equiv C-CH_2-Br + \Delta \rightarrow HC\equiv C\cdots CH_2 + Br$. The nozzle temperature varies from 300 to 1400 K. The molecular beam is photoionized by 118.2 nm laser light (10.487 eV), and the ions are analyzed with a reflectron TOF mass spectrometer.

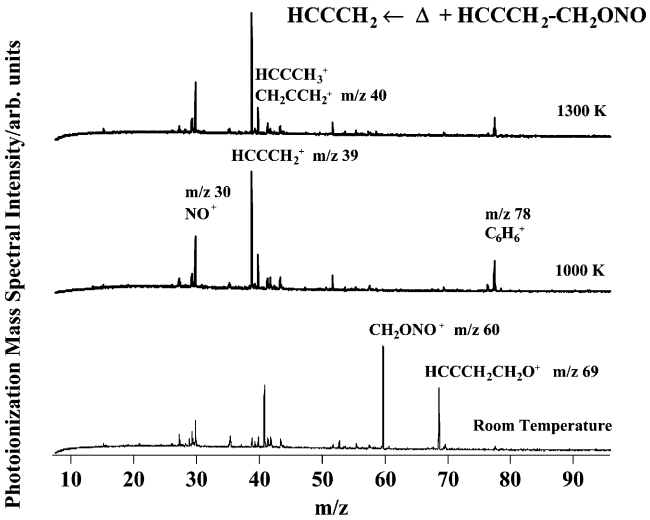

Figure 2. Photoionization mass spectra of the output of the hyperthermal nozzle; $HC\equiv C-CH_2-CH_2-O-N=O + \Delta \rightarrow HC\equiv C\cdots CH_2 + HCHO + NO$. The nozzle temperature varies from 300 to 1300 K. The molecular beam is photoionized by 118.2 nm laser light (10.487 eV), and the ions are analyzed with a reflectron TOF mass spectrometer.

K induces formation of NO, benzene, and $HC\equiv C\cdots CH_2$ as demonstrated by the ions at m/z 30, m/z 78, and m/z 39; the IE(HCHO) is 11.8 eV and HCHO cannot be ionized by the 118.2 nm VUV laser. At higher nozzle temperatures, ions derived from $CH_2=C=CH_2$ and $HC\equiv C-CH_3$ at m/z 40 are observed.

C. Assignments of the Propargyl Radical Infrared Spectra. The $HC\equiv C\cdots CH_2$ radicals are reactive species. Three contaminants that we always encounter in this work are benzene, $CH_2=C=CH_2$ and $HC\equiv C-CH_3$. This is consistent with the mass spectra shown in Figures 1 and 2, indicating that radical/radical dimerization and H-abstraction reactions are occurring in the hyperthermal nozzle.

Figures 3, 5, and 7 are the IR absorption spectra of propargyl radical in different wavelength regions. The experimental IR spectrum is the black trace and the assigned propargyl radical fundamentals are marked by bullets (•). Colored red and offset above the IR absorption spectrum are the DFT calculated harmonic frequencies $\{\omega\}_i$ [B3LYP/6-311G(d,p)] which are listed in Table 2. The predicted anharmonic frequencies resulting from the ab initio CCSD(T)/ANO calculation, $\{\upsilon\}_i$, are plotted as green sticks. A summary of our assignments for the fundamental vibrational modes of the propargyl radical, $\{\nu\}_i$,

TABLE 3: CH_2CCH $\tilde{X}$ $^2B_1$ Vibrational Modes in an Ar Matrix

			electronic structure calculation CCSD(T)/ANO		experimental frequencies Ar matrix		
mode		description	υ/cm^{-1}	A/km mol^{-1}	ν/cm^{-1}	A ratio/%	polarization
a_1	1	CH_2CC-H st	3322	51	3308.5 ± 0.5	100	negative
	2	sym $H_2C\cdots CCH$ st	3037	2	3028.3 ± 0.6	2	negative
	3	$CH_2C{=}CH - CH_2\cdots CCH$ st	1923	6	1935.4 ± 0.4	4	negative
	4	$H_2C\cdots CCH$ scissors	1444	0	1440.4 ± 0.5	2 ± 1	not available
	5	$CH_2C{=}CH \oplus CH_2\cdots CCH$ st	1055	4	1061.6 ± 0.8	7 ± 1	negative
b_1	6	$H_2C\cdots CCH$ umbrella	689	40	686.6 ± 0.4	44 ± 4	positive
	7	CH_2CC-H out-of-plane bend	482	51	483.6 ± 0.5	63 ± 7	positive
	8	$CH_2\cdots C{=}CH$ out-of-plane bend	398	5	not available		
b_2	9	asym $H_2C\cdots CCH$ st	3116	0	not available		
	10	$H_2C\cdots CCH \oplus CH_2-C{=}CH$ in-plane bend	1018	2	1016.7 ± 0.4	2	positive
	11	CH_2CC-H in-plane bend	612	47	620 ± 2	33 ± 4	positive
	12	$CH_2\cdots C{=}CH$ in-plane bend	338	5	not available		

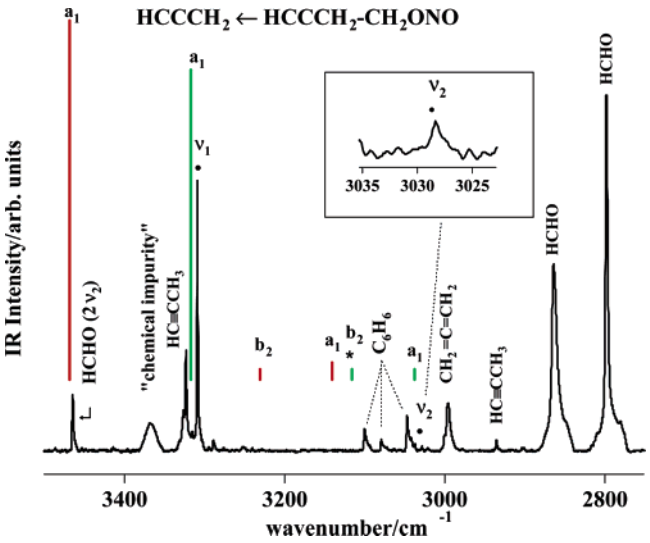

Figure 3. CH stretching region of the propargyl radical produced by thermal dissociation of $HC{\equiv}CCH_2CH_2ONO$. The DFT harmonic frequencies $\{\omega\}$ are shown as sticks in red, the CCSD(T) calculated anharmonic frequencies $\{\upsilon\}$ are shown as sticks in green, and the experimental fundamental frequencies $\{\nu\}$ are marked by bullets (•). The frequency ν_9 is predicted to be weak; so for display purposes we have enhanced its intensity by a factor of 10 and marked the scaled mode with *. The inset shows a tiny absorption at 3028.3 ± 0.6 cm^{-1} that we assign as ν_2. This band is just at the edge of our detection limit.

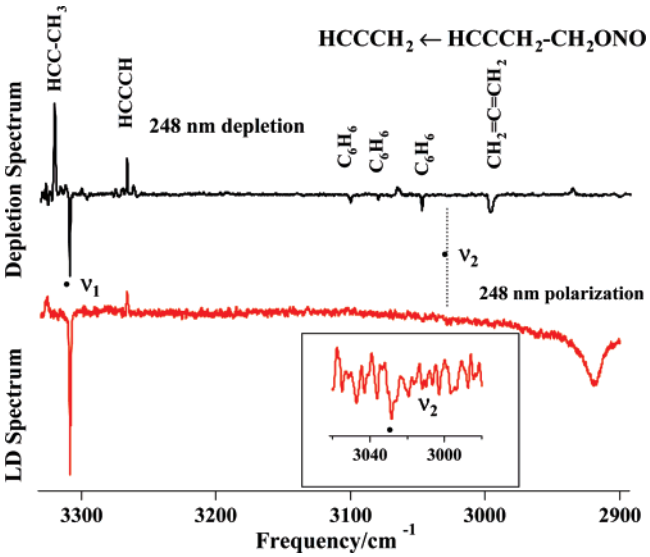

Figure 4. At the top (black) is the infrared spectrum following the depletion by 248 nm laser light of matrix isolated propargyl radicals produced by thermal dissociation of $HC{\equiv}CCH_2CH_2ONO$. On the bottom (red) is the linear dichroism spectrum of the propargyl radical following depletion by polarized 248 nm light. IR bands of propargyl that are a_1 polarized will have a negative dichroism whereas IR features with either b_1 or b_2 polarizations will have a positive dichroism. The ν_1 and ν_2 infrared fundamentals of the propargyl radical are both polarized a_1 and are marked by bullets (•).

is presented in Table 3. The CCSD(T) predictions for the anharmonic frequencies, $\{\upsilon\}_i$, are included for comparison.

Figure 3 is a scan of the CH stretching region of the infrared absorption spectrum. The propargyl radical, C_3H_3, must have three CH stretching fundamentals, but we only detect two of them. $\nu_1(HC{=}C\cdots CH_2)$, the intense acetylenic CH stretch, has been carefully studied in the gas phase,[17,18] in matrixes,[13−15] and on liquid He drops.[5] We observe this band at $\nu_1 = 3308.5 \pm 0.5$ cm^{-1}. The two methylene $-CH_2$ stretches are predicted (cf. Table 2) to be lower than ν_1. The symmetric $-CH_2$ stretch, ω_2 (a_1), is predicted to have a lower frequency than the asymmetric stretch, ω_9 (b_2). We only observe the weak symmetric CH stretch, shown in the inset, at $\nu_2 = 3028.3 \pm 0.6$ cm^{-1}.

The IR depletion spectrum and the LD spectrum for propargyl are shown in Figures 4, 6, and 8. A matrix of propargyl radicals was depleted by irradiation at 248 nm, exciting the dissociative[23] $\tilde{C}$ $^2B_1 \leftarrow \tilde{X}$ $^2B_1$ transition. Excitation of $HC{=}C\cdots CH_2$ radicals with a polarized laser beam at 248 nm depletes roughly 75% of the radicals, and consequently photoorients the matrix. By exciting to the $\tilde{C}$ $^2B_1$ dissociative state, radicals with a_1 transition moments $[\langle\tilde{C}\ ^2B_1|\mu|\tilde{X}\ ^2B_1\rangle]$ aligned with the laser are destroyed. This depleting laser light is horizontally polarized with respect to the laboratory frame, I_Z. Any molecule that has a significant projection of its transition dipole moment, $\mu_{a1}(\tilde{C} \leftarrow \tilde{X})$, parallel to the depleting laser light will be selectively depleted. The remaining $HC{=}C\cdots CH_2$ molecules will be oriented with their transition dipole moments perpendicular to the laboratory frame. Consequently if we measure the infrared linear dichroism spectrum ($I_Z - I_Y$) of the matrix, the a_1 modes will be depleted. That is, $I_Z - I_Y < 0$ (exhibit negative linear dichroism or LD) for levels of a_1 symmetry. Correspondingly, absorption intensities for b_1 and b_2 modes will be greater using horizontally oriented (Z direction) IR light for measurement; that is, $I_Z - I_Y > 0$ (exhibit positive linear dichroism or LD) for modes of b_1 or b_2 symmetry. By using the observed and calculated frequencies, and by matching the polarization spectra, we have assigned the $HC{=}C\cdots CH_2$ vibrations. We observe five vibrational transitions that have negative polarization and four features with a positive polarization.

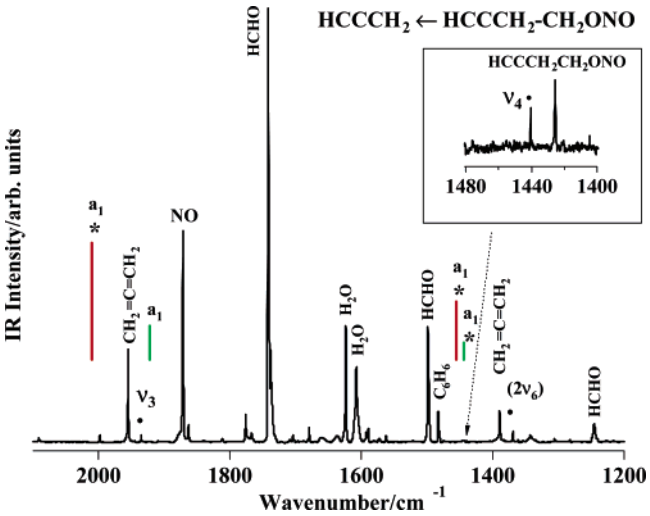

Figure 5. Fingerprint region of the propargyl radical produced by thermal dissociation of HC≡CCH$_2$CH$_2$ONO. The DFT harmonic frequencies {ω} are shown as sticks in red, the CCSD(T) calculated anharmonic frequencies {υ} are shown as sticks in green, and the experimental fundamental frequencies {ν} are marked by bullets (•). The frequencies {ω_3, ω_4, and ν_4} are predicted to be very weak. Hence for display purposes we have enhanced their intensities by a factor of 10 and marked the scaled modes with *. The small feature assigned as ν_4, the H$_2$C⋯CCH scissors mode, is predicted by both the DFT and CCSD(T) calculations to be around 1450 cm^{-1}; see Table 2. The inset shows a tiny absorption at 1440.4 ± 0.5 cm^{-1} that we assign as ν_4. This band is just at the edge of our detection limit.

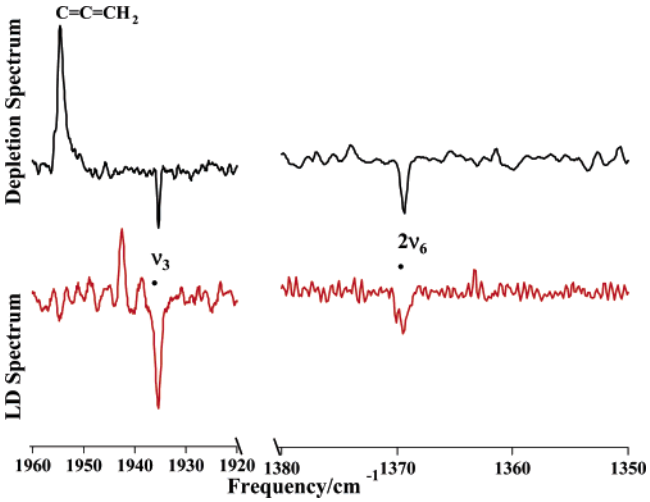

Figure 6. At the top (black) is the infrared spectrum following the depletion by 248 nm laser light of matrix isolated propargyl radicals produced by thermal dissociation of HC≡CCH$_2$CH$_2$ONO. On the bottom (red) is the linear dichroism spectrum of the propargyl radical following matrix depletion by polarized 248 nm light. The ν_3 infrared fundamental of the propargyl radical, the HC≐C⋯CH$_2$ stretching mode, is clearly polarized a$_1$ and is marked by bullet (•). The strong feature at 1369 cm^{-1} is polarized a$_1$ and originally we considered assigning it as ν_4. But the CCSD(T) calculations simply do not support such an assignment (see Figure 5). This band has been assigned as the overtone $2\nu_6$ of mode 6, the intense H$_2$C—CCH umbrella mode at 686 cm^{-1}. CCSD(T) calculations suggest that the 1369 cm^{-1} may be $2\nu_6$.

Figure 4 provides the IR depletion and LD spectra for the CH stretching region. Gas-phase rotational analysis[5,18] of the infrared band have conclusively demonstrated that the feature assigned as ν_1 is of a$_1$ symmetry. Figure 4 shows that two modes of the matrix-isolated HC≡C—CH$_2$ radical are depleted and both have a$_1$ symmetry. The 3028 cm^{-1} band that we assign to ν_2 is very weak; it is shown as an inset in Figure 4 and is barely detectable. Together Figures 3 and 4 enable us to assign the CH modes of propargyl to ν_1 and ν_2. These figures also unambiguously identify the presence of formaldehyde (HCHO), benzene (C$_6$H$_6$), allene (CH$_2$=C=CH$_2$), and methylacetylene (HC≡C—CH$_3$). The sharp feature at 3464 cm^{-1} in Figure 3 is the overtone[40] of ν_2 in formaldehyde; the broad band at 3367 cm^{-1} is an unknown chemical impurity. Photodissociation of the HC≐C⋯CH$_2$ radical leads to production of propargylene (HCCCH) and HC≡CCH$_3$.

One of the most interesting vibrations of the HC≐C⋯CH$_2$ radical is ν_3, the —C≐C— stretching mode. The vibrational frequency of a triple bond has a characteristic value in most organic molecules; this mode is observed[41] at 1974 cm^{-1} in HC≡CH and at 2147 cm^{-1} in CH$_3$C≡CH. Because of the conjugation in propargyl radical, one expects ν_3(HC≐C⋯CH$_2$) to be less than 2100 cm^{-1}. The CCSD(T) anharmonic calculated frequency, υ_3, is predicted (Table 2) at 1923 cm^{-1}, and is shifted from the corresponding harmonic prediction at 1983 cm^{-1}. In addition to the expected ν_3 mode, both DFT and CCSD(T) predict an additional, extremely weak mode, the $^{H}_{H}\rangle$C=⋯CCH scissoring mode υ_4, near 1450 cm^{-1}. Figure 5 shows two very weak modes of propargyl radical, which we assign as ν_3 = 1935.4 ± 0.4 cm^{-1} and ν_4 = 1440.4 ± 0.5 cm^{-1}.

Figure 6 is the comparison of the 248 nm depletion spectrum of HC≐C⋯CH$_2$ (eq 3) with the LD spectrum in this region. The ν_3 band of HC≐CCH$_2$ is clearly the feature at 1935.4 ± 0.4 cm^{-1} which is polarized a$_1$. We originally considered assigning the $^{H}_{H}\rangle$C=⋯CCH scissoring mode, ν_4 to the band at 1369 cm^{-1}. But the calculated frequencies in Table 3 clearly rule this out. The harmonic frequency ω_4 is calculated to be 1455 cm^{-1} and the CCSD(T) predicted ν_4 is 1444 cm^{-1}. Both transitions are calculated to be very weak; A_4 < 1 km mol^{-1}. Consequently, the experimental IR spectrum was carefully examined in the region of 1480−1400 cm^{-1}. An extremely weak band at 1440.4 ± 0.5 cm^{-1} (shown in the inset) was discovered, which we assign to ν_4 on the basis of the electronic structure calculations. The 1440 cm^{-1} feature is so weak that we cannot observe its depletion or polarization in Figure 6. The band at 1369 cm^{-1} was previously assigned[14] to the overtone ($2\nu_6$) of the intense b$_1$ $^{H}_{H}\rangle$C=⋯CCH umbrella-like mode, ν_6; we tentatively agree with this designation. The strong peak in the depletion spectrum is due to the very intense ν_2 mode of the propadienylidene[42] (CH$_2$=C=C), another photolysis product.

Figure 7 shows the fingerprint region of the spectrum, from 400−1200 cm^{-1}. Here we observe all five of the predicted modes of propargyl. The lowest frequency transition detected is at 483 cm^{-1} (ν_7). Although others[14] have assigned this peak to ν_{12} in the past, we identify the 483 cm^{-1} band with ν_7 on the basis of the electronic structure calculations as well as the depletion/LD spectra in Figure 8. The ν_7 mode corresponds to a CH out-of-plane-bend (b$_1$) which was observed earlier in the negative ion photodetachment spectra[7,8] at 490 ± 10 cm^{-1}.

Table 2 indicates that the pair of CH$_2$CC—H bending modes, ν_7 and ν_{11}, are simply related to each other. They are similar to the H—CC—H bending modes of acetylene[41] (π_g = 612 cm^{-1} and π_u = 730 cm^{-1}). Both the DFT and CCSD(T) calculations as well as the earlier CEPA-1 results predict the (ν_7, ν_{11}) pair to give rise to two relatively intense bands. We assign the peak at 620 cm^{-1} to be ν_{11}, the CH$_2$CC—H in-plane-bend, on the basis of the LD spectrum in Figure 8 and the calculations in Table 2. However, the 620 cm^{-1} band is unexpectedly weak. The LD spectrum in Figure 8 indicates that ν_{11} is polarized (b$_1$ or b$_2$) but it is not nearly as intense as ν_7. The ν_{11} band[43] in the depletion spectrum at the top of Figure 8 is not strong; the noisy portion of the depletion scan [encased by brackets] is a different

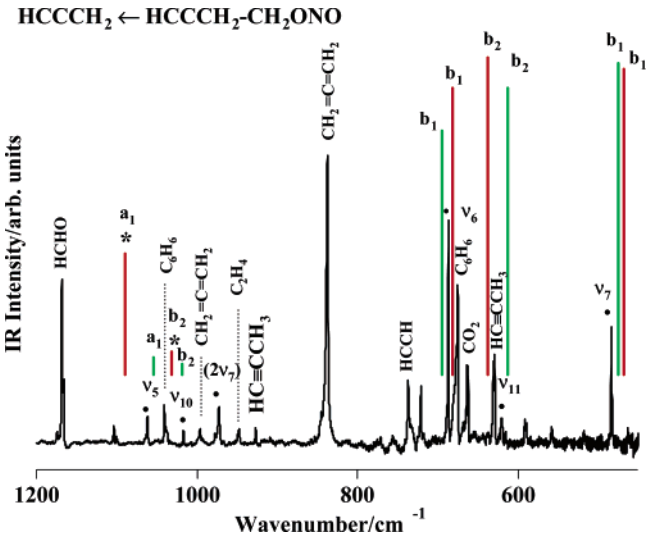

Figure 7. Fingerprint region of the propargyl radical produced by thermal dissociation of $HC{\equiv}CCH_2CH_2ONO$. The DFT harmonic frequencies $\{\omega\}$ are shown as sticks in red, the CCSD(T) calculated anharmonic frequencies $\{\upsilon\}$ are shown as sticks in green, and the experimental fundamental frequencies $\{\nu\}$ are marked by bullets (•). The harmonic frequencies, ω_5 and ω_{10}, are predicted to be very weak. Hence for display purposes we have enhanced their intensities by a factor of 10 and marked the scaled modes with *.

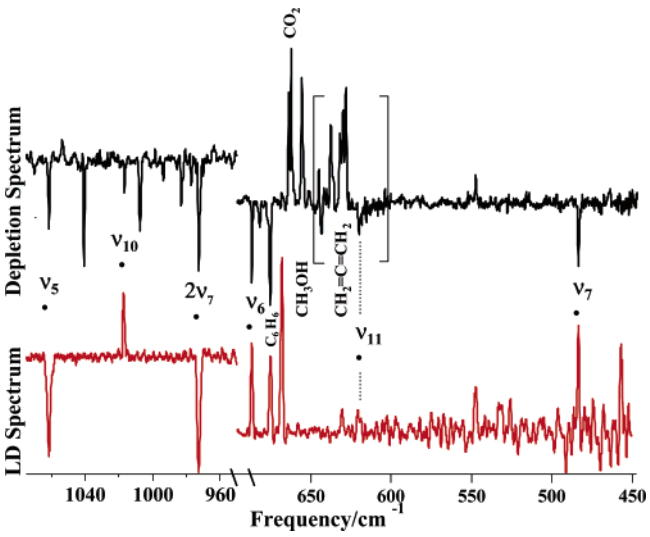

Figure 8. At the top (black) is the infrared spectrum following the depletion by 248 nm laser light of matrix isolated propargyl radicals produced by thermal dissociation of $HC{\equiv}CCH_2CH_2ONO$. On the bottom (red) is the linear dichroism spectrum of the propargyl radical following depletion by polarized 248 nm light. IR bands of propargyl that are a_1 polarized will have a negative dichroism whereas IR features with either b_1 or b_2 polarizations will have a positive dichroism. The ν_5, ν_{10}, ν_6, ν_{11}, and ν_7 infrared fundamentals of the propargyl radical are marked by bullets (•).

scan from the rest of Figure 8. The overtone of ν_7 ($2\nu_7$) is assigned to the relatively strong feature at 972 cm^{-1} on the basis of the CCSD(T) calculations that predict the intensity of this double quantum transition to be unusually large (approximately 10 km mol^{-1}). Figure 8 demonstrates that the 972 band is properly polarized a_1.

In gas-phase IR diode laser experiments,[16] unexpected bands were observed around 630 cm^{-1} for a series of lines which did not fit to the ν_6 band but had similar intensities. Tanaka et al. made a tentative assignment of these features to the $^pP_1$-branch lines of the ν_{11} band. The band origin of ν_{11} was estimated to be 647.3 cm^{-1}. This is a difficult assignment because of the strong perturbations by the *a*-type Coriolis interaction between the ν_{11} and ν_7 states. The gas-phase assignment[16] is 27 cm^{-1} higher than the ν_{11} matrix value shown in Figures 7 and 8.

The strong $^{H}_{H}\rangle C{=}{=}CCH$ umbrella mode, ν_6, at 686 cm^{-1} has been previously studied in both matrix[14] and gas-phase experiments.[16] Figure 8 demonstrates that the ν_6 mode is polarized as a (b_1 or b_2) mode. The band at 1017 cm^{-1} was previously assigned to ν_5, but this is not consistent with the LD spectra in Figure 8 and we assign it to ν_{10}, the $H_2C{\cdots}CCH$ bend. This also agrees well with the DFT and CCSD(T) calculations in Table 3. We believe that the feature at 1061 cm^{-1} is the ν_5 mode on the basis of linear dichroism spectroscopy (Figure 8). These values also agree better with the DFT and CCSD(T) calculations. The lowest frequency modes of propargyl radical, ν_8 and ν_{12} are not observed because they fall below the range of our MCT detector (415 cm^{-1}). The CCSD(T) calculations predict ν_8 at 398 cm^{-1} and ν_{12} at 338 cm^{-1}.

It is important to establish a complete set of internally consistent, reliable vibrational frequencies for the gas-phase propargyl radical. There are experimental gas-phase measurements for the three modes (ν_1, ν_6, and ν_7) and our matrix results, CCSD(T) calculations, and polarization measurements agree with these three assignments. Jacox has reviewed the matrix shifts for a large number of diatomic and small polyatomic free radicals and ions trapped in Ne and Ar matrixes.[44,45] She concluded that for polyatomic free radicals in Ar matrixes the frequency shift is generally less than 1% and usually to the red. Gas-phase vibrational frequencies[7,8,16,18,19] are available for three of propargyl's fundamentals: ν_1 (3322.2929 ± 0.0020 cm^{-1}), ν_6 (687.17603 ± 0.00062), and ν_7 (490 ± 10). The matrix values (from this study) are ν_1 (3308 cm^{-1}), ν_6 (686), and ν_7 (483). So for the propargyl radical, the gas-to-matrix shifts for these three modes are $\Delta\nu_1$ (14 cm^{-1}), $\Delta\nu_6$ (1 cm^{-1}), and $\Delta\nu_7$ (7 cm^{-1}). Consequently, we believe that all of the matrix frequencies for the propargyl radical are within 1% of the true, gas-phase frequencies. [In an earlier study of the allyl radical,[46] we observed the five CH streching modes. High-resolution laser

TABLE 4: Recommended Gas-Phase Vibrational Frequencies for $HC{\equiv}C{\cdots}CH_2$ $\tilde{X}$ $^2B_1$

mode		description	ν/cm^{-1}	method	ref
a_1	1	$CH_2CC{-}H$ st	3322.2929 ± 0.0020	CW color center laser spectroscopy	17, 18
	2	sym $H_2C{\cdots}CCH$ st	3028 ± 15	Ar matrix, CCSD(T) calculation	this work
	3	$CH_2C{\equiv}CH - CH_2{\cdots}CCH$ st	1935 ± 15	Ar matrix, CCSD(T) calculation	this work
	4	$H_2C{\cdots}CCH$ scissors	1440 ± 15	Ar matrix, CCSD(T) calculation	this work
	5	$CH_2C{\equiv}CH \oplus CH_2{\cdots}CCH$ st	1061 ± 15	Ar matrix, CCSD(T) calculation	this work
b_1	6	$H_2C{\cdots}CCH$ umbrella	687.17603 ± 0.00062	time resolved IR diode laser spectroscopy	16
	7	$CH_2CC{-}H$ out-of-plane bend	490 ± 10	$CH_2{=}C{=}CH^-$ photodetachment	7, 8
	8	$CH_2{\cdots}C{\equiv}CH$ out-of-plane bend	396 ± 15	CCSD(T) calculation	this work
b_2	9	asym $H_2C{\cdots}CCH$ st	3124 ± 15	Ar matrix, CCSD(T) calculation	14
	10	$H_2C{\cdots}CCH \oplus CH_2{-}C{\equiv}CH$ in-plane bend	1017 ± 15	Ar matrix, CCSD(T) calculation	this work
	11	$CH_2CC{-}H$ in-plane-bend	620 ± 30	Ar matrix, CCSD(T) calculation	this work
	12	$H_2C{\cdots}C{\equiv}CH$ in-plane bend	352 ± 15	CCSD(T) calculation	this work

spectroscopy[47] subsequently detected all five of the CH_2CHCH_2 fundamentals. For allyl radical, the gas-to-matrix shifts were found: $\Delta\nu_1$ (25 cm^{-1}), $\Delta\nu_2$ (18 cm^{-1}), $\Delta\nu_3$ (4 cm^{-1}), $\Delta\nu_{13}$ (4 cm^{-1}), and $\Delta\nu_{14}$ (0 cm^{-1}).]

Consequently, we will use matrix shifts in the ν_1, ν_6, and ν_7 modes to estimate the gas-to-matrix shifts and uncertainties for the rest of the bands. In Table 4 we have collected a set of gas-phase vibrational frequencies that we recommend be adopted for the $HC{\equiv}C{\cdots}CH_2$ $\tilde{X}\ ^2B_1$ radical. In constructing Table 4, we have to deal with ν_{11}. We clearly observe this b_2 mode in absorption (Figure 7) from two different precursors as well as in the depletion/LD spectra (Figure 8) at $\nu_{11} = 620 \pm 2$ cm^{-1}. The ab initio CCSD(T) anharmonic value that we found for this mode was $\upsilon_{11} = 612$ cm^{-1} (Table 3). However, Tanaka et al.[16] made a tenative assignment for the origin of ν_{11} at 647.3 cm^{-1}. Either there is a huge gas-to-matrix shift for ν_{11} or one of the experimental assignments is incorrect. Therefore we recommend the value of $\nu_{11} = 620 \pm 30$ cm^{-1}; the unusually large uncertainty covers the matrix spectra in Figures 7 and 8, the CCSD(T) calcuated anharmonic mode, and the tenative assignment of Tanaka et al.[16]

IV. Discussion

The PIMS spectra in Figures 1 and 2 indicate that a pulsed hyperthermal jet is a reliable source of the $HC{\equiv}C{\cdots}CH_2$ radical for spectroscopic studies. Both the PIMS spectra as well as the infrared spectra (Figures 3, 5, and 7) show that a fraction of the propargyl radicals dimerize in the nozzle to form benzene. Propargyl also abstracts H atoms at either end of $HC{\equiv}C{\cdots}CH_2$ to produce both methylacetylene and allene: $C_3H_3 \rightarrow \{C_6H_6, CH_3C{\equiv}CH$, and $CH_2{=}C{=}CH_2\}$. Figures 4 and 6 also demonstrate that upon irradiation with 248 nm photons, $HC{\equiv}C{\cdots}CH_2$ photofragments to H and propargylene or propadienylidene: $HC{\equiv}C{\cdots}CH_2 + \hbar\omega_{248nm} \rightarrow H + HC{=}C{=}CH$ or $CH_2{=}C{=}C$.

The nature and extent of electron delocalization in propargyl is an interesting question. Figure 9 is an isosurface ($\rho = 0.01$ e a_0^{-3}) of the CCSD(T)/ANO calculated spin density. The calculated electron spin is delocalized on the (1,3) carbons as found earlier by experimental EPR spectroscopy;[3] see eq 1. Atomic partitioning of the calculated density in Figure 9 finds 35% of the spin on C(3) and 65% on C(1).

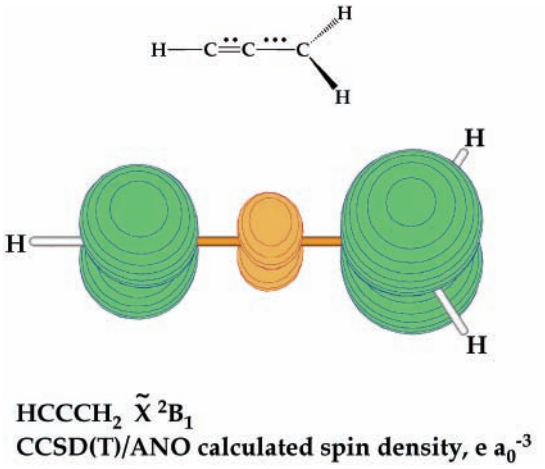

Figure 9. Plot of the CCSD(T)/ANO spin density ($\rho = 0.01$ e a_0^{-3}) calculated for the $\tilde{X}\ ^2B_1$ state of $HCCCH_2$. The regions in green represent excess α spin, and the yellow regions indicate an excess of β spin. The coefficients in eq 6 are based on an atomic partitioning of the spin using Mulliken populations. At this contour level the small amount of β spin on the hydrogens is not seen.

The small electric dipole moment[5] of propargyl is related to the extensive electron delocalization in the radical. Table 5 collects some of the properties of $CH_3{-}C{\equiv}C{-}H$ and $CH_2{=}C{=}CH_2$. The observed[5] dipole moment of the radical is much closer to allene than methylacetylene: $[\mu_D{}^{\delta-}(HCCCH_3)^{\delta+} = 0.784 \pm 0.001$ D] > $[\mu_D{}^{\delta-}(HC{\equiv}C{\cdots}CH_2)^{\delta+} = 0.150 \pm 0.005$ D] > $[\mu_D(CH_2{=}C{=}CH_2) = 0$ D]. The structure for $HC{\equiv}C{\cdots}CH_2$ has not been experimentally determined but the computed CCSD(T)/ANO geometry in Table 2 is certainly a very good estimate.

TABLE 5: Properties of Methylacetylene and Allene for Comparison

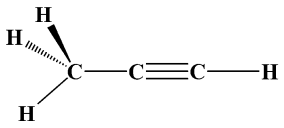

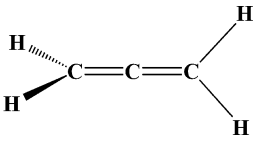

	methylacetylene		allene[48]	
	$r(CH_3CC{-}H)$/Å	1.105	$r(CH_2CCH{-}H)$	1.085
	$r(H{-}CH_2CCH)$/Å	1.056		
	$r(CH_3C{\equiv}CH)$/Å	1.206	$r(CH_2{=}CCH_2)$	1.309
	$r(CH_3{-}CCH)$/Å	1.459		
	$\theta(H{-}CH_2{-}CCH)$/deg	110.2	$\theta(H{-}CH{=}C{=}CH_2)$/deg	120.2
	$\mu_D{}^{\delta+}(CH_3CCH)^{\delta-}$/D	0.784 ± 0.001	$\mu_D(CH_2CCH_2)$/D	0[50,51]

	modes of $CH_3C{\equiv}CH$ (C_{3v})			modes of $CH_2{=}C{=}CH_2$ (D_{2d})[41]			
mode		description	ν/cm^{-1}	mode		description	ν/cm^{-1}
$a_1(z)$	1	C−H st	3334	a_1	1	CH_2 sym st	3015
	2	CH_3 sym st	2918		2	CH_2 sym scissors	1443
	3	C≡C st	2142		3	C=C sym st	1073
	4	CH_3 sym def	1382				
	5	C−C st	931	b_1	4	CH_2 twist	865
e(*x*,*y*)	6	CH_3 deg st	3008	$b_2(z)$	5	CH_2 asym st	3007
	7	CH_3 deg def	1452		6	C=C asym st	1957
	8	CH_3 rock	1053		7	CH_2 asym scissors	1398
	9	C−H bend	633				
	10	CCC bend	328	e(x,y)	8	CH_2 asym st	3086
					9	CH_2 rock	999
					10	CH_2 wag	841
					11	CCC def	355

Comparison with the allene and methylacetylene structures in Table 5 indicates that the structure of propargyl radical is truly intermediate between methylacetylene and allene; eq 5 compares the CC bond lengths (Å).

$$\underset{\mathrm{HC{\equiv}C{-}CH_3}}{\overset{1.206\quad 1.459}{}} \qquad \underset{\mathrm{HC{\cdot\cdot}C{\cdot\cdot\cdot}CH_2}}{\overset{1.228\quad 1.380}{}} \qquad \underset{\mathrm{CH_2{=}C{=}CH_2}}{\overset{1.309\quad 1.309}{}} \tag{5}$$

Recall[48] that $r_e(HC{\equiv}CH) = 1.207$ Å and $r_e(CH_2{=}CH_2) = 1.339$ Å.

We can represent the propargyl radical with the generalized valence band formula[49] in eq 6. The coefficients in (6) are based on an atomic partitioning of the CCSD(T)/ANO spin density using Mulliken populations.

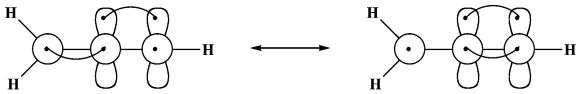

35 % $\tilde{X}\ ^2B_1$ CH_2CCH (propargyl radical) 65 % (6)

The calculated structure of the propargyl radical in Table 2 and eq 5 certainly predicts a hydrocarbon radical with a long CC bond and a short CC bond. However, the delocalized GVB structure in eq 6 is supported by the small dipole moment, $\mu_D(HC{\doteq}C{\cdot\cdot\cdot}CH_2) = 0.150 \pm 0.005$ D, and by the strongly coupled CC stretching vibrations. Table 5 collects the vibrational frequencies for $HC{\equiv}C{-}CH_3$ and $CH_2{=}C{=}CH_2$. The two modes in methylacetylene, $\nu_3(HC{\equiv}CCH_3) = 2142$ cm^{-1} and $\nu_5(HCC{-}CH_3) = 931$ cm^{-1}, are clearly separate, local modes. In contrast, the pair of double bonds in allene are strongly coupled as the pair $\nu_3(CH_2{=}C{=}CH_2$, sym st$) = 1073$ cm^{-1} and $\nu_6(CH_2{=}C{=}CH_2$, asym st$) = 1957$ cm^{-1}. The CC stretching modes of propargyl, $\nu_3(HC{\doteq}C{\cdot\cdot\cdot}CH_2$, asym st$) = 1935$ cm^{-1} and $\nu_5(HC{\doteq}C{\cdot\cdot\cdot}CH_2$, sym st$) = 1062$ cm^{-1}, in Table 3 seem to mirror $CH_2{=}C{=}CH_2$ much more than $HC{\equiv}C{-}CH_3$.

There is a striking resemblance of propargyl, $HC{\doteq}C{\cdot\cdot\cdot}CH_2$ $\tilde{X}\ ^2B_1$, to allyl, $CH_2{\cdot\cdot\cdot}CH{\cdot\cdot\cdot}CH_2$ $\tilde{X}\ ^2A_2$. Both are strongly delocalized, C_{2v} π radicals, as shown by the molecular structures; eq 5 for $HC{\doteq}C{\cdot\cdot\cdot}CH_2$ and the microwave structure for $CH_2{\cdot\cdot\cdot}CH{\cdot\cdot\cdot}CH_2$ reported in ref 46. The resonance energy[12] is roughly 11 kcal mol^{-1} for each of these hydrocarbons. Both radials have small electric dipole moments,[5] $\mu_D(HC{\doteq}C{\cdot\cdot\cdot}CH_2) = 0.150$ D vs $\mu_D(CH_2{\cdot\cdot\cdot}CH{\cdot\cdot\cdot}CH_2) = 0.07$ D. The vibrational modes of both allyl[46] and propargyl (Table 4) are not easily described by local modes but more naturally by a set of vibrations delocalized over the entire molecule. Because of its symmetry, the allyl radical must be described by an equal mixture of two GVB structures, eq 7. Such is nearly the case for propargyl, eq 6.

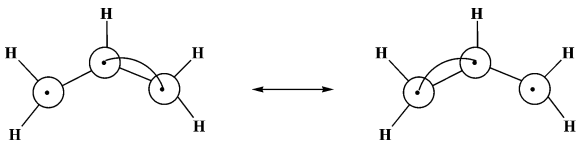

50 % $\tilde{X}\ ^2A_2$ CH_2CHCH_2 (allyl radical) 50 % (7)

Acknowledgment. The research in Colorado was supported by grants from the Chemical Physics Program, United States Department of Energy (DE-FG02-87ER13695) and the National Science Foundation (CHE-9813659). J.F.S. and M.E.V. thank the NSF and Welch Foundations.

References and Notes

(1) Flood, W. E. *The Dictionary of Chemical Names*; Littlefield, Adams, & Co.: Totowa, NJ, 1967. The propargyl radical is derived from propargyl alcohol, $HClCCH_2OH$. Like acetylene, propargyl alcohol and related compounds form complexes with silver and copper. The name propargyl is derived from *prop(ionic)* [chain of three carbon atoms] + *arg-(entum)* [Latin for silver].

(2) Hahn, D. K.; Klippenstein, S. J.; Miller, J. A. *Faraday Discuss.* **2001**, *119*, 79.

(3) Kasai, P. H. *J. Am. Chem. Soc.* **1972**, *94*, 5950.

(4) Tanaka, K.; Sumiyoshi, Y.; Ohshima, Y.; Endo, Y.; Kawaguchi, K. *J. Chem. Phys.* **1997**, *107*, 2728.

(5) Küpper, J.; Merritt, J. M.; Miller, R. E. *J. Chem. Phys.* **2002**, *117*, 647.

(6) Minsek, D. W.; Chen, P. *J. Phys. Chem.* **1990**, *94*, 8399.

(7) Oakes, J. M.; Ellison, G. B. *J. Am. Chem. Soc.* **1983**, *105*, 2969.

(8) Robinson, M. S.; Polak, M. L.; Bierbaum, V. M.; Depuy, C. H.; Lineberger, W. C. *J. Am. Chem. Soc.* **1995**, *117*, 6766.

(9) Berkowitz, J.; Ellison, G. B.; Gutman, D. *J. Phys. Chem.* **1994**, *98*, 2744.

(10) Ellison, G. B.; Davico, G. E.; Bierbaum, V. M.; DePuy, C. H. *Int. J. Mass Spectrom. Ion Processes* **1996**, *156*, 109.

(11) Blanksby, S. J.; Ellison, G. B. *Acc. Chem. Res.* **2003**, *36*, 255.

(12) Notice that this makes the resonance stabilization energy of the propargyl radical to be about that of allyl radical; see: Ellison; et. al. *Int. J. Mass Spectrom. Ion Processes* 1996. Comparing propene [$\Delta H_{298}(CH_2{-}CHCH_2{-}H) = 88.8 \pm 0.4$ kcal mol^{-1}], methylacetylene [$\Delta H_{298}(HCCCH_2{-}H) = 90 \pm 3$ kcal mol^{-1}], ethane [$\Delta H_{298}(CH_3CH_2{-}H) = 101.1 \pm 0.4$ kcal mol^{-1}], one finds resonance energy(CH_2CHCH_2) = 12 kcal mol^{-1} and resonance energy($HCCCH_2$) = 11 kcal mol^{-1}.

(13) Jacox, M. E.; Milligan, D. E. *Chem. Phys.* **1974**, *4*, 45.

(14) Korolev, F. A.; Mal'tsev, A. K.; Nefedov, O. M. *Bull. Acad. Sci. USSR Div. Chem. Sci.* **1989**, *38*, 957.

(15) Huang, J. W.; Graham, W. R. M. *J. Chem. Phys.* **1990**, *93*, 1583.

(16) Tanaka, K.; Harada, T.; Sakaguchi, K.; Harada, K.; Tanaka, T. *J. Chem. Phys.* **1995**, *103*, 6450.

(17) Morter, C. L.; Domingo, C.; Farhat, S. K.; Cartwright, E.; Glass, G. P.; Curl, R. F. *Chem. Phys. Lett.* **1992**, *195*, 316.

(18) Yuan, L.; DeSain, J.; Curl, R. F. *J. Mol. Spectrosc.* **1998**, *187*, 102.

(19) Eckhoff, W. C.; Miller, C. E.; Billera, C. F.; Engel, P. S.; Curl, R. F. *J. Mol. Spectrosc.* **1997**, *186*, 193.

(20) Ramsay, D. A.; Thistlethwaite, P. *Can. J. Phys.* **1966**, *44*, 1381.

(21) Honjou, H.; Yoshimine, M.; Pacansky, J. *J. Phys. Chem.* **1987**, *91*, 4455.

(22) Wyss, M.; Riaplov, E.; Maier, J. P. *J. Chem. Phys.* **2001**, *114*, 10355.

(23) Fahr, A.; Hassanzadeh, P.; Laszlo, B.; Huie, R. E. *Chem. Phys.* **1997**, *215*, 59.

(24) Zhang, X.; Friderichsen, A. V.; Nandi, S.; Ellison, G. B.; David, D. E.; McKinnon, J. T.; Lindeman, T. G.; Dayton, D. C.; Nimlos, M. R. *Rev. Sci. Instrum.* **2003**, *74*, 3077.

(25) Pedley, J. B.; Naylor, R. D.; Kirby, S. P. *Thermochemistry of Organic Compounds*, 2nd ed.; Chapman and Hall: New York, 1986. The heats of formation for CH_3ONO, CH_3O, and NO are known. Consequently the bond enthalpy for methylnitrite is $\Delta H_{298}(CH_3O{-}NO) = 42.0 \pm 0.7$ kcal mol^{-1}.

(26) Pugh, L. A.; Narahari Rao, K. Intensities From Infrared Spectra. In *Molecular Spectroscopy: Modern Research*; Rao, K. N., Ed.; Academic Press: New York, 1976; Vol. II, p 165. The units of *A* are frequently puzzling. The frequency is always in wavenumbers, cm^{-1}. If the IR cross section, σ, is reported in units of cm^2 molecule^{-1}, then the units of *A* are cm molecule^{-1}. *A*/cm molecule^{-1} implies that the target density is *n*/molecules cm^{-3} and the path length is *z*/cm. If one used *n*/atm and *z*/cm, then *A* will have the units *A*/cm^{-2} atm^{-1}. The SI unit for *A* uses *n*/mol cm^{-3} and *z*/cm, so one has *A*/cm mol^{-1} or *A*/km mol^{-1}. Most electronic structure programs use the SI unit for *A* and lists them as km mol^{-1}; this is the manner in which we have reported *A* in Table 2.

(27) Becke, A. D. *J. Chem. Phys.* **1993**, *98*, 5648.

(28) Lee, C. T.; Yang, W. T.; Parr, R. G. *Phys. Rev. B* **1988**, *37*, 785.

(29) Lee, T. J.; Scuseria, G. E. In *Quantum Mechanical Electronic Structure Calculations with Chemical Accuracy*; Langhoff, S. R., Ed.; Kluwer: Dordrecht, 1995.

(30) Bartlett, R. J. In *Modern Electronic Structure Theory, Part II*; Yarkony, D. R., Ed.; World Scientific: Singapore, 1995.

(31) Gauss, J. Coupled Cluster Theory. In *Encyclopedia of Computational Chemistry*; Schleyer, P., Ed.; Wiley: New York, 1998.

(32) Crawford, T. D.; Schaefer, H. F., III. *Rev. Comput. Chem.* **1999**, *14*, 36.

(33) Raghavachari, K.; Trucks, G. W.; Pople, J. A.; Head-Gordon, M. *Chem. Phys. Lett.* **1989**, *157*, 479.

(34) Raghavachari, K.; Trucks, G. W.; Pople, J. A.; Replogle, E. *Chem. Phys. Lett.* **1989**, *158*, 207.

(35) Almlof, J.; Taylor, P. R. *J. Chem. Phys.* **1987**, *86*, 4070.

(36) Watts, J. D.; Gauss, J.; Bartlett, R. J. *J. Chem. Phys.* **1993**, *98*, 8718.

(37) Stanton, J. F.; Lopreore, C. L.; Gauss, J. *J. Chem. Phys.* **1998**, *108*, 7190.

(38) Mulliken, R. S. *J. Chem. Phys.* **1955**, *23*, 1997. The IUPAC recommends that C_{2v} objects always be orientated with the *x* axis out of the molecular plane. We adopt Herzberg's convention (*Molecular Spectra and Molecular Structure: Infrared and Raman Spectra of Polyatomic Molecules*; D. Van Nostrand: Princeton, NJ, 1945; p 271) for numbering the fundamental vibrational modes. Modes are numbered from highest to lowest with ν_1 belonging to the highest frequency in the totally symmetric block. Subsequent modes are numbered down the lower symmetric blocks.

(39) Botschwina, P.; Oswald, R.; Flügge, J.; Horn, M. *Z. Phys. Chem.-Int. J. Res. Phys. Chem. Chem. Phys.* **1995**, *188*, 29.

(40) Nelander, B. *J. Chem. Phys.* **1980**, *73*, 1026.

(41) Shimanouchi, T. *Tables of Molecular Vibrational Frequencies, Consolidated Vol. I*; National Bureau of Standards: Washington, DC, 1972; Vol. I (NSRDS-NBS 39).

(42) Seburg, R. A.; Patterson, E. V.; Stanton, J. F.; McMahon, R. J. *J. Am. Chem. Soc.* **1997**, *119*, 5847.

(43) We do not fully understand the rather anomalous features of ν_{11}. It is both more broad and considerably less intense than expected on the basis of ν_7. That these features are not due to matrix effects is clear from the gas-phase study of $CH_2{=}C{=}O$, where the oddly weak (as compared with theoretical predictions) nature of the feature tentatively assigned as ν_{11} was noted.

(44) Jacox, M. E. *J. Mol. Spectrosc.* **1985**, *113*, 286.

(45) Jacox, M. E. *Chem. Phys.* **1994**, *189*, 149.

(46) Nandi, S.; Arnold, P. A.; Carpenter, B. K.; Nimlos, M. R.; Dayton, D. C.; Ellison, G. B. *J. Phys. Chem. A* **2001**, *105*, 7514.

(47) Han, J. X.; Utkin, Y. G.; Chen, H. B.; Hunt, N. T.; Curl, R. F. *J. Chem. Phys.* **2002**, *116*, 6505.

(48) Harmony, M. D.; Laurie, V. W.; Kuczkowski, R. L.; Schwendeman, R. H.; Ramsay, D. A.; Lovas, F. J.; Lafferty, W. J.; Maki, A. G. **1979**, *8*, 619.

(49) Goddard, W. A., III.; Harding, L. B. *Annu. Rev. Phys. Chem.* **1978**, *29*, 363

(50) Blake, T. A.; Eggers, D. F.; Tseng, S. H.; Lewerenz, M.; Swift, R. P.; Beck, R. D.; Watts, R. O.; Lovas, F. *J. Chem. Phys.* **1993**, *98*, 6031.

(51) Tan, X. Q.; Xu, L. W.; Tubergen, M. J.; Kuczkowski, R. L. *J. Chem. Phys.* **1994**, *101*, 6512.

(52) Zierhut, M.; Noller, B.; Schultz, T.; Fischer, I. *J. Chem. Phys.*, in press.